

# Uncertainty Quantification in Discrete Fracture Network Models

CLAUDIO CANUTO

Dipartimento di Scienze Matematiche, Politecnico di Torino  
claudio.canuto@polito.it

Joint work with

STEFANO BERRONE, SANDRA PIERACCINI, STEFANO SCIALÒ  
(DISMA, Politecnico di Torino)

AMCS Seminar - KAUST, 10 February 2014

## 1 Introduction

- New approach: a PDE optimization problem

## 2 Discretization

- The discrete problem

## 3 Some numerical experiments

- Stochastic fracture transmissivity
  - Test 1
  - Test 2
  - Test 3
- Stochastic geometry (work in progress)

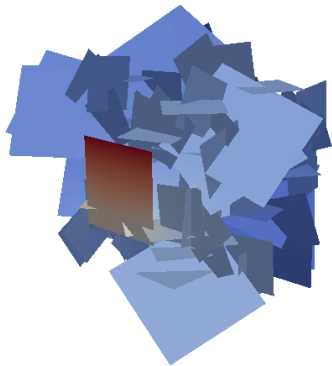
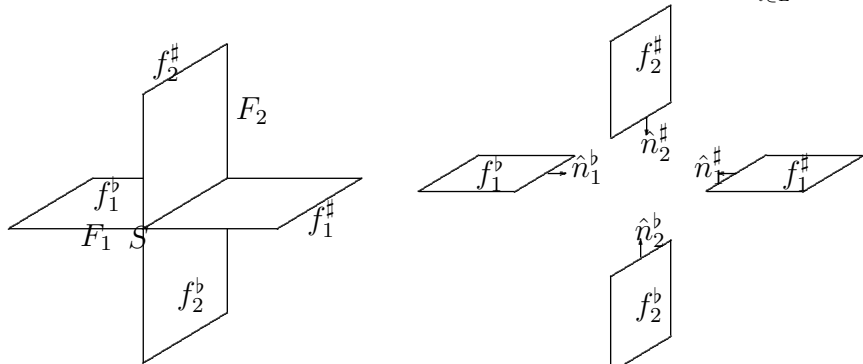


Figure: Example of DFN

Discrete fracture network models:

- 3D network of intersecting fractures
- Fractures are represented as planar polygons
- Rock matrix is considered impervious
- Quantity of interest is the hydraulic head evaluated with Darcy law
- Flux balance and hydraulic head continuity imposed across trace intersections

- The computational domain is denoted  $\Omega = \bigcup_{i \in I} F_i$ ,  $\partial\Omega = \bigcup_{i \in I} \partial F_i$ .
- $F_i \subset \mathbb{R}^3$ ,  $i \in I$  is a generic fracture of the system;
- Fracture intersections are called *traces* and denoted by  $S_m$ ,  $m \in M$ ;
- Each trace is a set of non-vanishing segments that are shared by exactly two fractures:  $S_m = \bar{F}_i \cap \bar{F}_j$ , and  $I_{S_m} = \{i, j\}$ ;
- $\mathcal{S}_i$  is the set of traces on fracture  $F_i$  while  $\mathcal{S}$  denotes the set of all the traces;
- $f_l \subset \mathbb{R}^3$ ,  $l \in L$  is a generic sub-fracture, obtained splitting fractures  $F_i$  in such a way that each trace is contained in the boundary of the sub-fractures.  $\Omega = \bigcup_{l \in L} \bar{f}_l \setminus \partial\Omega$



The global hydraulic head  $H$  in  $\Omega$  is provided by the solution of the following coupled problems  $\forall l \in L$  with a 2D local reference system on  $f_l$  expressing the Darcy law:

$$\begin{aligned} -\nabla \cdot (\mathbf{K}_{f_l} \nabla H) &= q, & \text{in } f_l, \\ H|_{\Gamma_D \cap \partial f_l} &= H_D, & \text{on } \Gamma_D \cap \partial f_l, \\ \frac{\partial H}{\partial \hat{\nu}_{\partial f_l}} &= H_N, & \text{on } \Gamma_N \cap \partial f_l. \end{aligned}$$

plus additional coupling conditions: let  $L_{S_m} = \{l : S_m \subset \partial f_l\}$ , then

$$\begin{aligned} H|_{\bar{f}_l} &= H|_{\bar{f}_k} \text{ on } S_m, & \forall S_m \in \mathcal{S}, \quad \forall l, k \in L_{S_m}, \\ \sum_{l \in L_{S_m}} \frac{\partial H|_{\bar{f}_l}}{\partial \hat{\nu}_{\partial f_l}} &= 0 \text{ on } S_m, & \forall S_m \in \mathcal{S}. \end{aligned}$$

Here,

$$\frac{\partial H}{\partial \hat{\nu}} := \hat{n} \cdot (\mathbf{K} \nabla H).$$

Let us denote by  $H_i$  the restriction of  $H$  to the fracture  $F_i$ ,  $\forall i \in I$ . The previous compatibility conditions can be written as:

$$\begin{aligned} H_i|_{S_m} - H_j|_{S_m} &= 0, & \text{for } i, j \in I_{S_m}, \forall m \in M, \\ \left[ \left[ \frac{\partial H_i}{\partial \hat{\nu}_{S_m}^i} \right] \right]_{S_m} + \left[ \left[ \frac{\partial H_j}{\partial \hat{\nu}_{S_m}^j} \right] \right]_{S_m} &= 0, & \text{for } i, j \in I_{S_m}, \forall m \in M, \end{aligned}$$

where  $\left[ \left[ \frac{\partial H_i}{\partial \hat{\nu}_{S_m}^i} \right] \right]_{S_m}$  denotes the jump of the co-normal derivative along the unique normal  $\hat{n}_{S_m}^i$  fixed for the trace  $S_m$  on the fracture  $F_i$ . This jump is independent of the orientation of  $\hat{n}_{S_m}^i$ .

**Remark.** We assume  $q \in L^2(f_l)$ , so that the conormal derivative is well-defined in  $H^{-\frac{1}{2}}(\partial f_l)$ .

## Proposition

Let

$$U_i^{S_m} := \left[ \left[ \frac{\partial H_i}{\partial \hat{\nu}_S^i} \right] \right]_S \quad U_i^{S_m} \in \mathcal{U}^S = H^{-\frac{1}{2}}(S), \quad \forall S \in \mathcal{S}$$

and  $U_i \in \mathcal{U}^{S_i}$  the tuple of functions  $U_i^S \quad \forall S \in \mathcal{S}_i$ .

Let further be  $\partial F_i = \Gamma_{iN} \cup \Gamma_{iD}$  with  $\Gamma_{iN} \cap \Gamma_{iD} = \emptyset$  and  $\Gamma_{iD} \neq \emptyset$ .

Then, solving  $\forall i \in I$  the problem:

find  $H_i = H_i^0 + \mathcal{R} H_{iD}$ , with  $H_i^0 \in V_i := H_{D,0}^1(F_i)$  such that:

$$\begin{aligned} (\mathbf{K} \nabla H_i^0, \nabla v) &= (q_i, v) + \langle U_i, v|_{S_i} \rangle_{\mathcal{U}^{S_i}, \mathcal{U}^{S_i'}} + \langle H_{iN}, v|_{\Gamma_{iN}} \rangle_{H^{-\frac{1}{2}}(\Gamma_{iN}), H^{\frac{1}{2}}(\Gamma_{iN})} \\ &\quad - (\mathbf{K} \nabla \mathcal{R} H_{iD}, \nabla v), \quad \forall v \in V_i \end{aligned}$$

with additional conditions

$$\begin{aligned} H_i|_{S_m} - H_j|_{S_m} &= 0, & \text{for } i, j \in I_{S_m}, \quad \forall m \in M, \\ U_i^{S_m} + U_j^{S_m} &= 0, & \text{for } i, j \in I_{S_m}, \quad \forall m \in M, \end{aligned}$$

is equivalent to solve the problems on the subfractures.

[Berrone, Pieraccini and Scialò (SISC2013a-b, JCP2014)]

Instead of solving the coupled differential problems on the fractures or sub-fractures with the corresponding matching conditions we look for the solution solving a PDE constrained optimal control problem, the variable  $U$  being the control variable. Let us define the differentiable quadratic functional  $J : \mathcal{U} \rightarrow \mathbb{R}$  as

$$J(U) = \sum_{S \in \mathcal{S}} \left( \|H_i(U_i)|_S - H_j(U_j)|_S\|_{\mathcal{H}^S}^2 + \|U_i^S + U_j^S\|_{\mathcal{U}^S}^2 \right)$$

variable  $U$  being the tuple of all control variables  $U_i$ .

## Proposition

Let us define the spaces  $\mathcal{U}^S$  and  $\mathcal{H}^S$  as

$$\mathcal{U}^S = H^{-\frac{1}{2}}(S), \quad \mathcal{H}^S = H^{\frac{1}{2}}(S) = \mathcal{U}^{S'}$$

then the hydraulic head  $H \in H_D^1(\Omega)$  is the unique exact solution of DFN problem if and only if it satisfies the differential problems on  $F_i$ ,  $\forall i \in I$  and correspondingly  $J(U) = 0$ .

## Definition of the discrete problem

- Introduce a finite element triangulation on each fracture, completely independent of the triangulation on the intersecting fractures. Let us further define on this triangulation a finite element discretization  $h$  for  $H$ .
- Introduce also a discretization  $u$  for the control variable  $U$ , on the traces of each fracture independently.
- Let us choose  $\mathcal{U}^S = \mathcal{H}^S = L^2(S)$  for the discrete norms

Then we have

- Algebraic formulation of quadratic functional:  $J(u, h) = \frac{1}{2}h^T G^h h + \frac{1}{2}u^T G^u u$
- Algebraic formulation of PDE constraints:  $A_i h_i - B_i u = \tilde{q}_i, \quad i \in I.$

Grouping the matrices  $A_i$  and  $B_i$  in the matrices  $A$  and  $B$ , and  $\tilde{q}_i$  in  $\tilde{q}$  the problem becomes

$$\begin{aligned} \min_{u, h} \quad & J(u, h) := \frac{1}{2}h^T G^h h + \frac{1}{2}u^T G^u u \\ \text{s.t.} \quad & Ah - Bu = \tilde{q}. \end{aligned}$$

**Note:**  $h$  denotes the discretized head, in the sequel the mesh-size will be denoted by  $\delta$ .

# The unconstrained problem

Use the linear constraint to remove  $h$  from  $J$ :

$$\begin{aligned} J(u, h(u)) &= \frac{1}{2} (A^{-1}(Bu + \tilde{q}))^T G^h (A^{-1}(Bu + \tilde{q})) + \frac{1}{2} u^T G^u u \\ &= \frac{1}{2} u^T (B^T A^{-T} G^h A^{-1} B + G^u) u + u^T B^T A^{-T} G^h A^{-1} \tilde{q} + \frac{1}{2} \tilde{q}^T A^{-T} G^h A^{-1} \tilde{q} \end{aligned}$$

such that the minimum of the constrained problem is the same as the solution to the unconstrained problem:

$$\min \hat{J}(u), \quad \hat{J}(u) := \frac{1}{2} u^T (B^T A^{-T} G^h A^{-1} B + G^u) u + u^T B^T A^{-T} G^h A^{-1} \tilde{q}$$

that can be solved by a gradient-based method. The gradient of  $\hat{J}$  in a point  $\bar{u}$  is:

$$\nabla \hat{J}(\bar{u}) = B^T p + G^u \bar{u}$$

where

$$p_i = A_i^{-T} G_i^h h_i \quad \text{and} \quad h_i = A_i^{-1} (B_i \bar{u}_i - \tilde{q}_i)$$

with

$$h = (h_1, \dots, h_{\#I})^T \quad \text{and} \quad p = (p_1, \dots, p_{\#I})^T.$$

Let us observe that, given a value to the control variables  $\bar{u}_i$ ,  $\forall i \in I$  only LOCAL problems on each fracture are solved in order to evaluate the gradient.

# Main advantages of the proposed method

- The numerical triangulation for the discrete solution is fully independent of each fracture and trace
- the gradient method makes the optimization approach to DFN simulations nearly *inherently parallel*
- on a multicore or GPU architecture we can associate each fracture to a different core
- exchange of very small amount of data between processes
- each process only exchanges data with a limited number of other known processes
- resolution of small linear systems independently performed

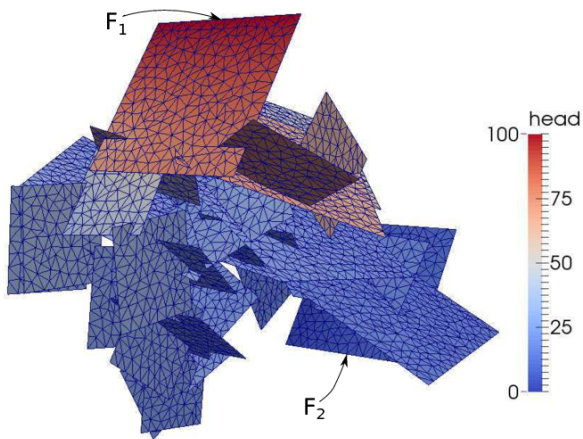
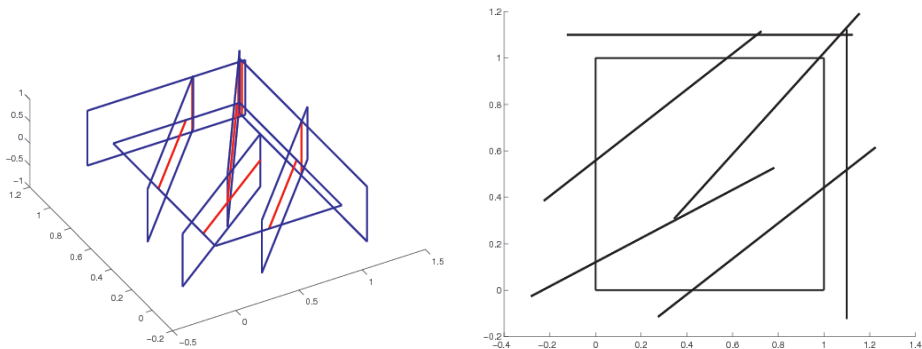


Figure: An example of mesh on a DFN

# A toy network for our numerical experiments



**Figure:** An example of toy network. Left: 3D view of the network (traces in red); right: projection on  $x_1$ - $x_2$  plane

We consider several toy networks with:

- 1 An horizontal fracture  $F_1$
- 2 Two vertical orthogonal fractures  $F_2, F_3$  (with reference to previous 2D figure:  $F_2$  on the right of  $F_1$ ,  $F_3$  above  $F_1$ )
- 3 A set of additional fractures connecting the network, orthogonal to  $F_1$ , and with arbitrary orientation.

Boundary conditions:

- 1 The east edge of  $F_1$  acts as a source (Neumann boundary conditions set to 10)
- 2 On south edge of  $F_2$  and east edge of  $F_3$  (constant non-homogeneous) Dirichlet b.c. are set
- 3 All other edges are assumed to be insulated: homogenous Neumann conditions.

We consider the problem of measuring the overall flux entering fractures  $F_2$  and  $F_3$  through their traces, respectively.

- DFN simulations are largely interesting in those situations in which the discrete nature of the fractures strongly impacts on the directionality of the flow.
- DFN are usually applied to simulate the underground displacement of pollutant, water or super-critical carbon dioxide. The simulations mainly aim at estimating the flux entity, the resulting directionality of the flux, and characteristic time.
- In this context we assume as characteristic quantity the flux that is affecting a fixed boundary of the DFN (fractures  $F_2$  and  $F_3$ ).
- A possible scenario is as follows:
  - Assume information is available about the probability distribution of certain fracture features, such as their density, orientation, size, aspect ratio, aperture (these data may affect transmissivity).
  - Assume a borehole is pumping some fluid underground (e.g., carbon dioxide)
  - We are interested in evaluating the probability that the flux of carbon dioxide reaches a certain region of the underground basin, where a large outcropping fault can be a carrier for a dangerous leakage.

- Non intrusive methods  
(a MUST in our application, due to the computational cost of each realization, performed by an iterative solver)
- Stochastic collocation approach
- Gauss-Patterson grids in each direction  
(to re-use expensive information from previous levels)
- Smolyak-type sparse grids for multi-dimensional stochastic variables
- A vast literature on such strategy is available since mid 2000's, including more recent insights in Nonlinear Approximation and Adaptivity  
[Babuška, Tempone, Nobile, Webster, Xiu, Hesthaven, Tamellini, Schwab, DeVore, ...].

- 1 Test 1: Same transmissivity  $K$  on all fractures:

$$K = 10^{L_{\min} + (L_{\max} - L_{\min})Y}, \quad Y \sim \mathcal{U}(0, 1)$$

- 2 Test 2: Different transmissivities  $K_i$  on the fractures:

$$K_1 = K_2 = K_3 = 10^{\bar{L}}, \quad K_i = 10^{L_{\min} + (L_{\max} - L_{\min})Y_i}, \quad Y_i \sim \mathcal{U}(0, 1)$$

for  $i = 4, \dots, N$ , with  $Y_i$  independent random variables.

- 3 Test 3: Different transmissivities  $K_i$ , dictated by a KL expansion:

$$K_1 = K_2 = K_3 = 10^\mu, \quad K_i = 10^{L_i} \quad \text{with} \quad L_i = L_0 + \sum_{n=1}^{\infty} \sqrt{\lambda_n} \phi_n(\mathbf{x}_{B_i}) Y_n(\omega)$$

for  $i = 4, \dots, N$ , where  $\mathbf{x}_{B_i}$  is the center of mass of  $F_i$ .

# Test 1

We consider  $\#I = 7$  fractures. On each fracture,

$$K = 10^{L_{\min} + (L_{\max} - L_{\min})Y}, \quad Y \sim \mathcal{U}(0, 1)$$

with  $L_{\min} = -4$ ,  $L_{\max} = 0$ .

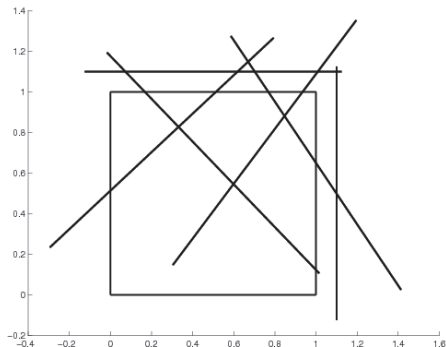


Figure: DFN configuration for Test 1

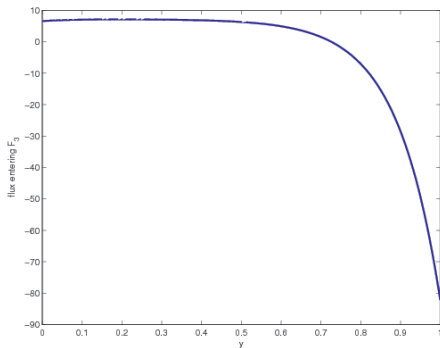
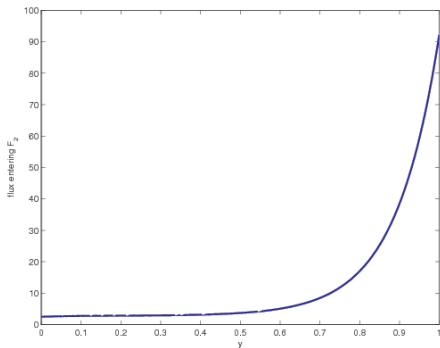


Figure: Flux entering  $F_2$  (left) and  $F_3$  (right) versus  $y$

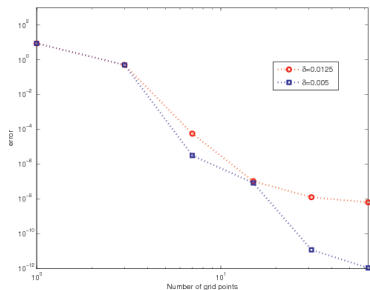
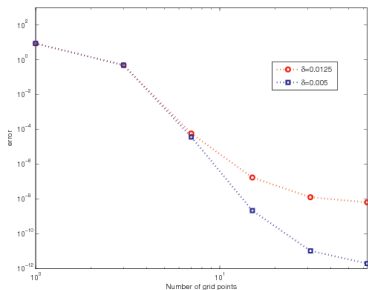
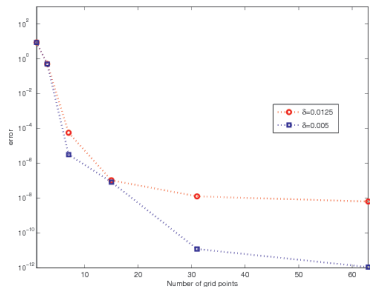
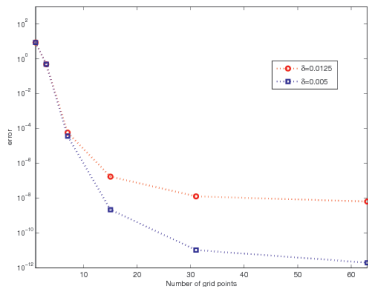


Figure: Mean value errors for flux entering  $F_2$  (left) and  $F_3$  (right) versus number of grid points (Gauss-Patterson grid). Top: semi-log scale; bottom: log-log scale

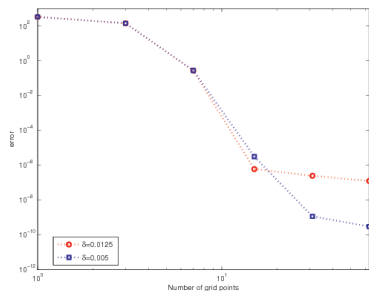
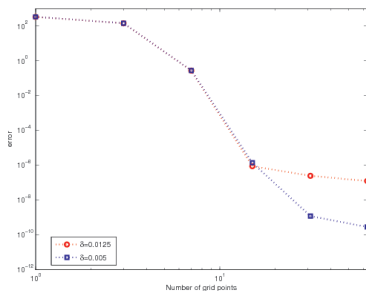
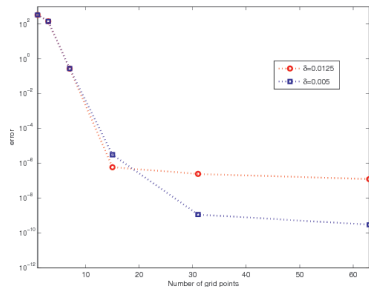
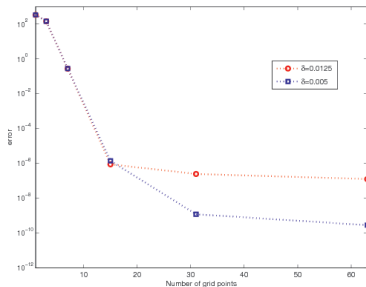


Figure: Variance errors for flux entering  $F_2$  (left) and  $F_3$  (right) versus number of grid points (Gauss-Patterson grid). Top: semi-log scale; bottom: log-log scale

We consider  $\#I = 7$  fractures. We set

$$K_1 = K_2 = K_3 = 10^{\bar{L}}, \quad K_i = 10^{L_{\min} + (L_{\max} - L_{\min})Y_i}, \quad Y_i \sim \mathcal{U}(0, 1)$$

for  $i = 4, \dots, N$ , with  $L_{\min} = -4$ ,  $L_{\max} = 0$ ,  $\bar{L} = -2$ .

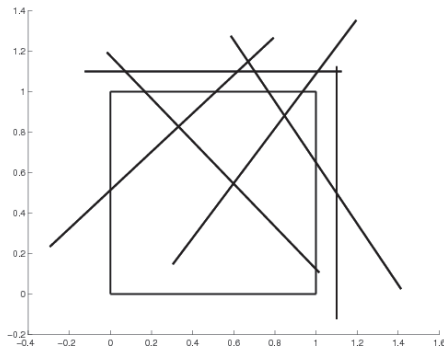
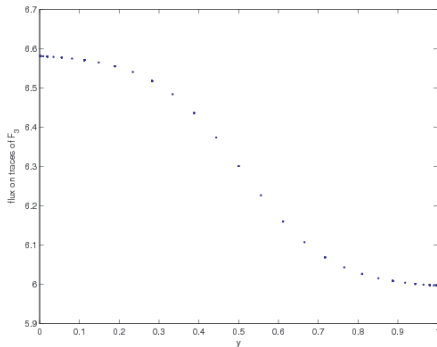
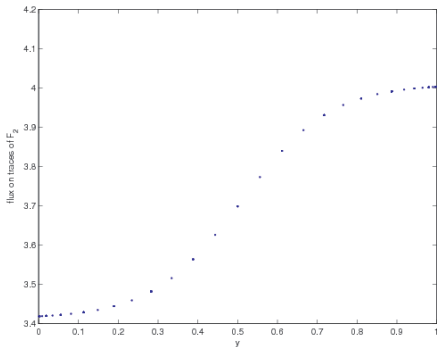


Figure: DFN configuration for Test 2 (same as for Test 1)



**Figure:** Flux entering  $F_2$  (left) and  $F_3$  (right) versus one selected stochastic variable  $y_i$ , the one associated with the fracture with smallest distance from the intersection  $F_2 \cap F_3$  (all others set to 0.5)

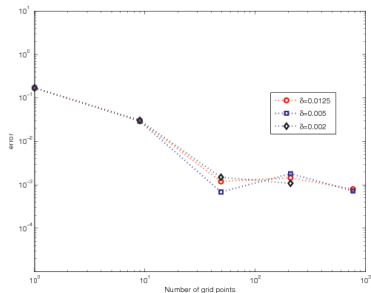
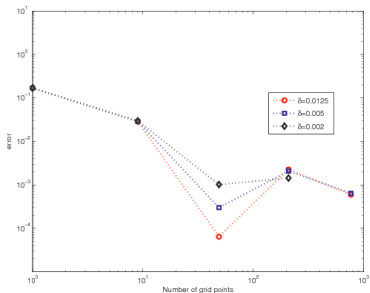
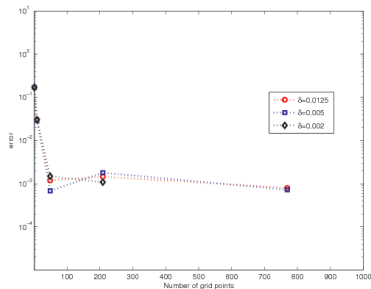
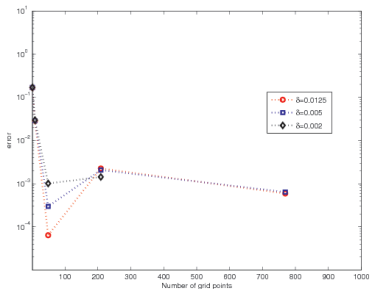


Figure: Mean value errors for flux entering  $F_2$  (left) and  $F_3$  (right) versus number of grid points (Gauss-Patterson sparse grid). Top: semi-log scale; bottom: log-log scale

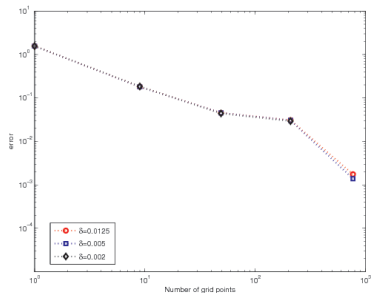
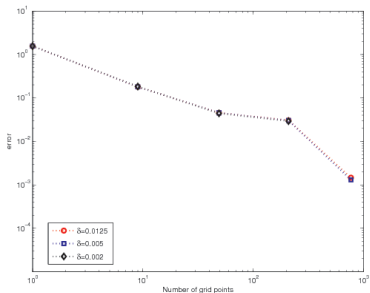
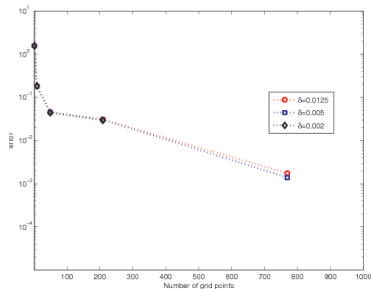
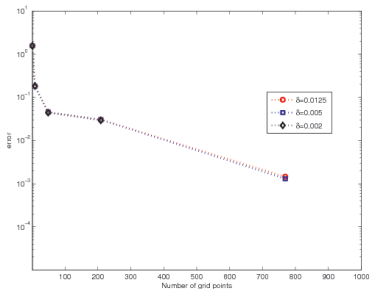


Figure: Variance errors for flux entering  $F_2$  (left) and  $F_3$  (right) versus number of grid points (Gauss-Patterson sparse grid). Top: semi-log scale; bottom: log-log scale

We consider  $\#I = 12$  fractures. We set  $K_1 = K_2 = K_3 = 10^{-2}$  and for  $i = 4, \dots, N$

$$K_{i,M} = 10^{L_{i,M}}, \quad L_{i,M} = L_0 + \sum_{n=1}^M \sqrt{\lambda_n} \phi_n(\mathbf{x}_{B_i}) Y_n(\omega).$$

The Karhunen-Loève decomposition is computed with a covariance function

$$C_L(\mathbf{x}, \mathbf{z}) = e^{-\frac{\|\mathbf{x}-\mathbf{z}\|^2}{\gamma^2}}, \quad \mathbf{x}, \mathbf{z} \in D$$

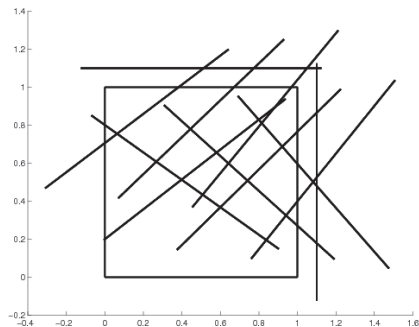


Figure: DFN configuration for Test 3

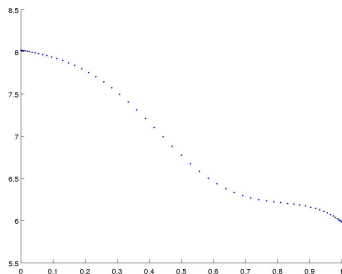


Figure: Flux entering  $F_2$  versus the stochastic variable  $y_1$ ;  $\gamma = 1.5$

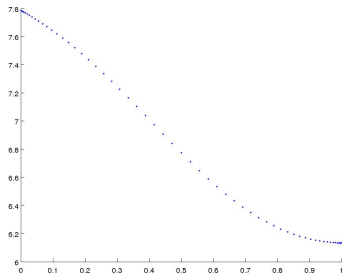
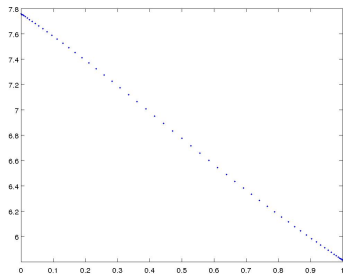
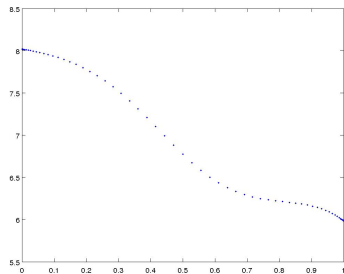
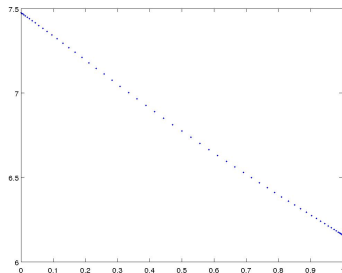
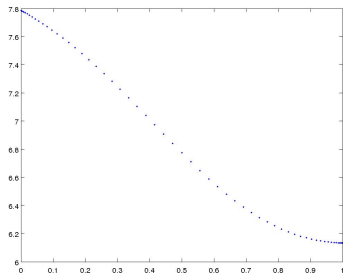


Figure: Flux entering  $F_2$  versus the stochastic variable  $y_1$ ;  $\gamma = 0.25$



**Figure:** Flux entering  $F_2$  versus the stochastic variables  $y_1$  (left;  $y_2 = 0.5$ ) and  $y_2$  (right;  $y_1 = 0.5$ );  $\gamma = 1.5$



**Figure:** Flux entering  $F_2$  versus the stochastic variables  $y_1$  (left;  $y_2 = 0.5$ ) and  $y_2$  (right;  $y_1 = 0.5$ );  $\gamma = 0.25$

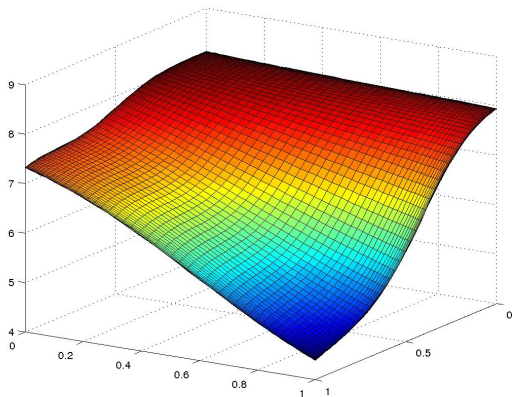


Figure: Flux entering  $F_2$  versus the stochastic variables  $y_1$  and  $y_2$ ;  $\gamma = 1.5$

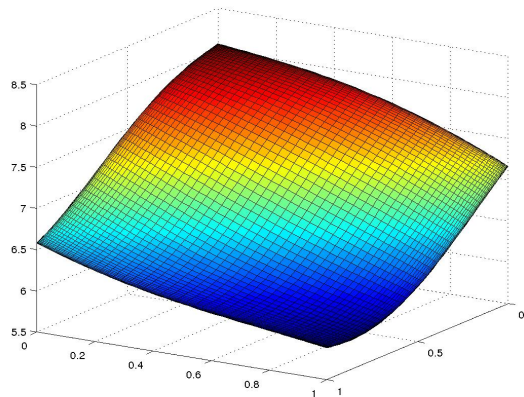


Figure: Flux entering  $F_2$  versus the stochastic variables  $y_1$  and  $y_2$ ;  $\gamma = 0.25$

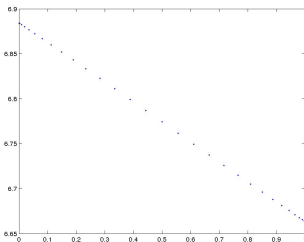
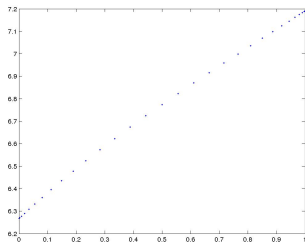
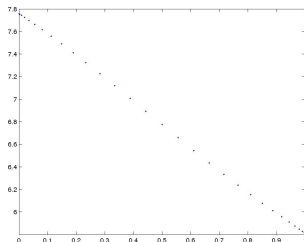
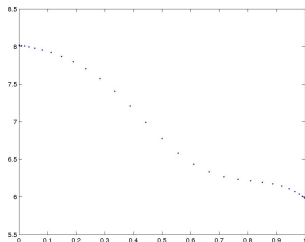


Figure: Left to right, top to bottom: flux entering  $F_2$  versus the stochastic variables  $y_1$ ,  $y_2$ ,  $y_3$ ,  $y_4$  respectively. All others set to 0.5;  $\gamma = 1.5$ .

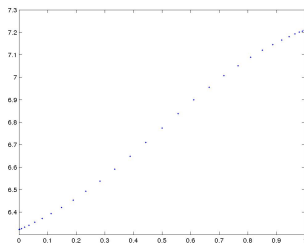
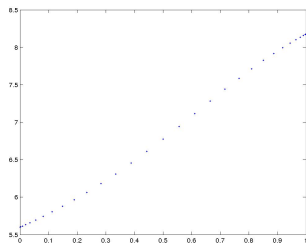
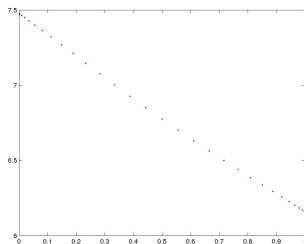
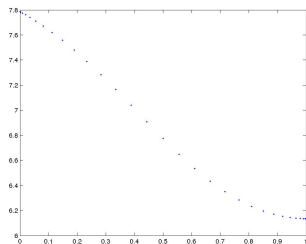
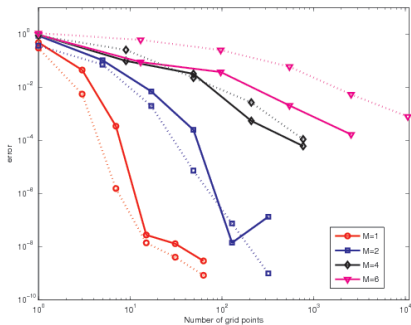
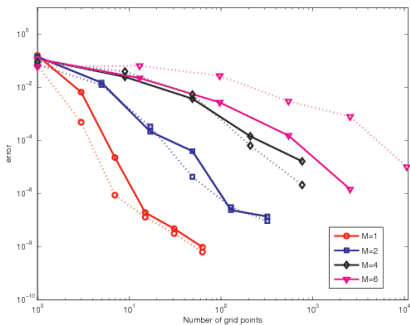


Figure: Left to right, top to bottom: flux entering  $F_2$  versus the stochastic variables  $y_1$ ,  $y_2$ ,  $y_3$ ,  $y_4$  respectively. All others set to 0.5;  $\gamma = 0.25$ .



**Figure:** Mean value (left) and variance (right) errors for flux entering  $F_2$  versus number of grid points (Gauss-Patterson sparse grid). Solid line:  $\gamma = 1.5$ , dotted line:  $\gamma = 0.25$ .

Similar behaviours reported in the literature (e.g., [Nobile, Tempone and Webster \(2008\)](#)).

We consider a geometry in which the orientation of the fractures is non-deterministic.  $K$  is fixed for all fractures.

Fracture  $F_i$ , for  $i \geq 4$ , forms an angle  $\alpha_i$  with the  $x_1$  axis which is

$$\alpha_i = \bar{\alpha}_i + \Delta\alpha_i(2y - 1), \quad y \sim \mathcal{U}(0, 1).$$

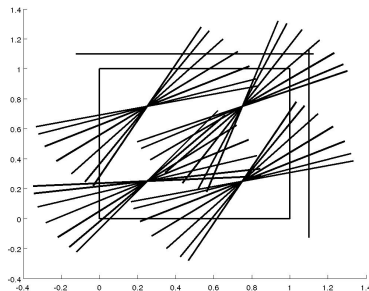


Figure: Non-deterministic configuration.

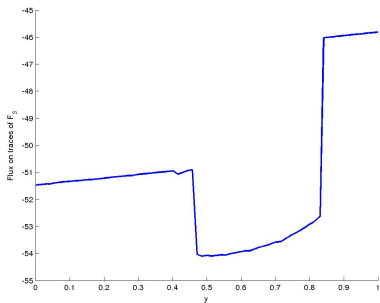
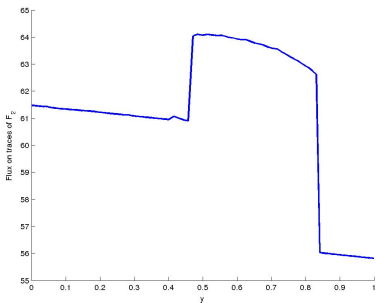


Figure: Flux entering  $F_2$  (left) and  $F_3$  (right) versus the stochastic variable  $y$

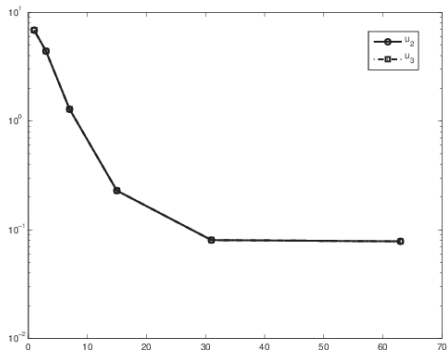
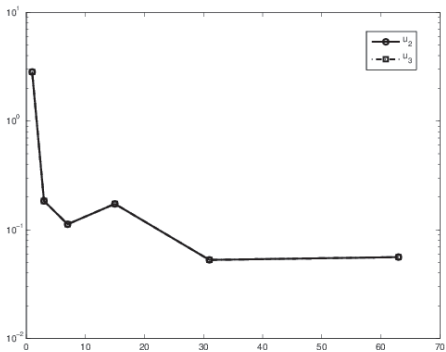


Figure: Errors on mean value (left) and variance (right) versus number of grid points

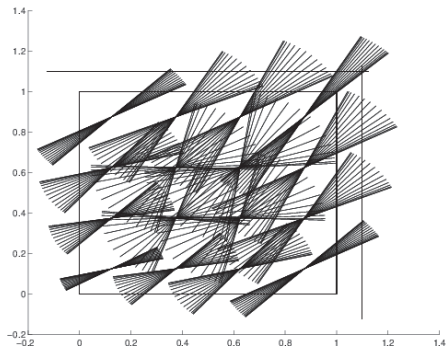


Figure: Non-deterministic configuration: increasing number of fractures.

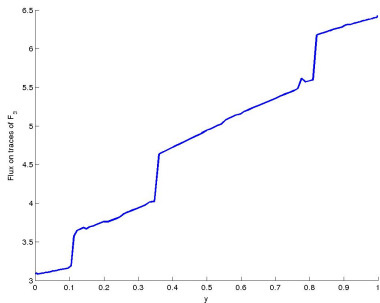
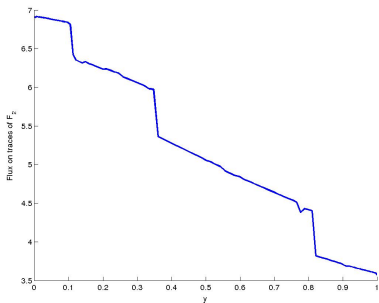


Figure: Flux entering  $F_2$  (left) and  $F_3$  (right) versus the stochastic variable  $y$

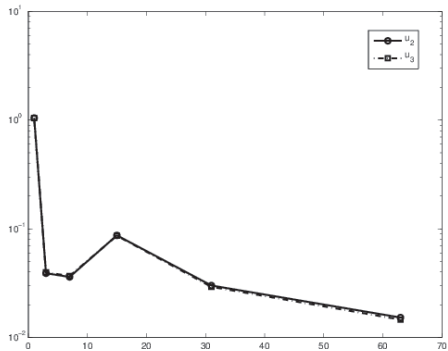
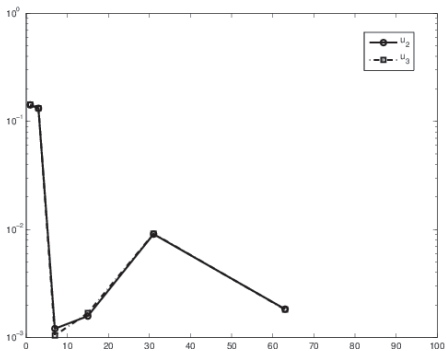


Figure: Errors on mean value (left) and variance (right) versus number of grid points

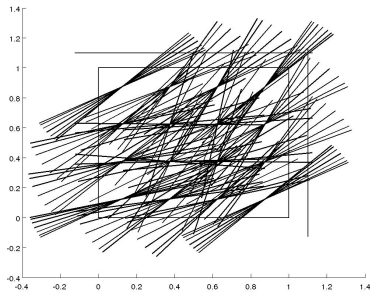


Figure: Non-deterministic configuration: increasing some fractures' length.

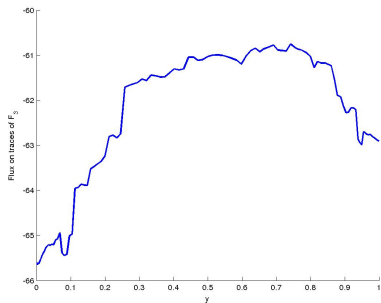
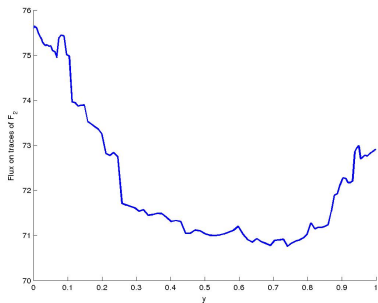


Figure: Flux entering  $F_2$  (left) and  $F_3$  (right) versus the stochastic variable  $y$

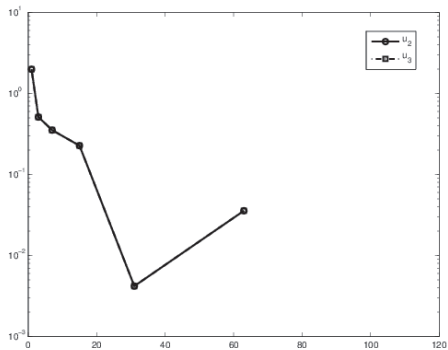
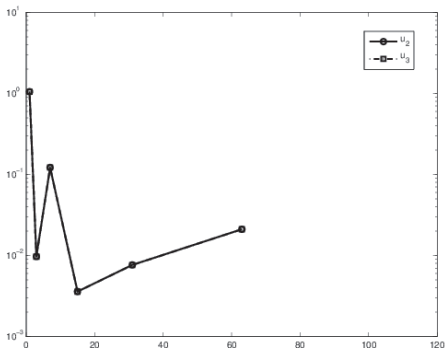


Figure: Errors on mean value (left) and variance (right) versus number of grid points

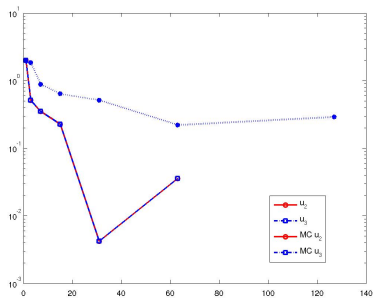
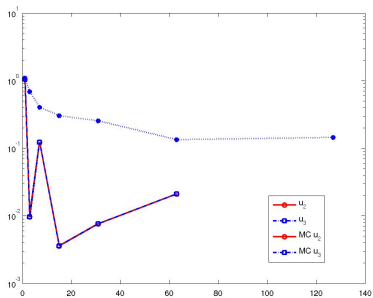


Figure: Errors on mean value (left) and variance (right) versus number of grid points. Stochastic collocation (solid lines) vs Monte Carlo (dotted lines)

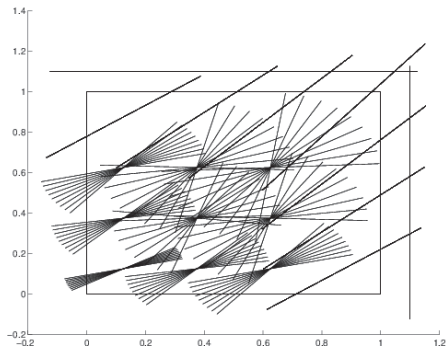


Figure: Non-deterministic configuration: non-deterministic orientation only for inner fractures.

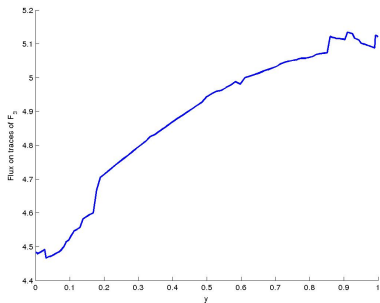
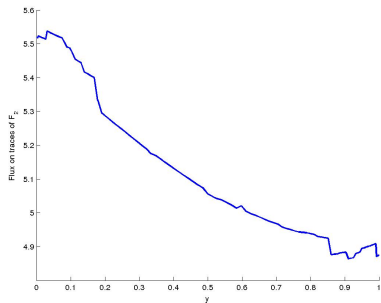


Figure: Flux entering  $F_2$  (left) and  $F_3$  (right) versus the stochastic variable  $y$

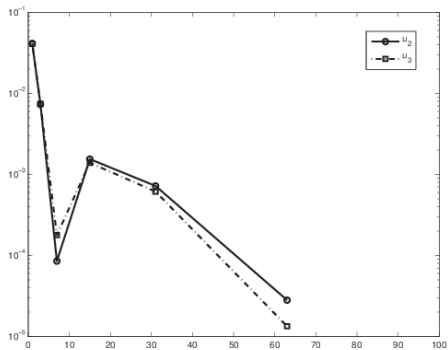
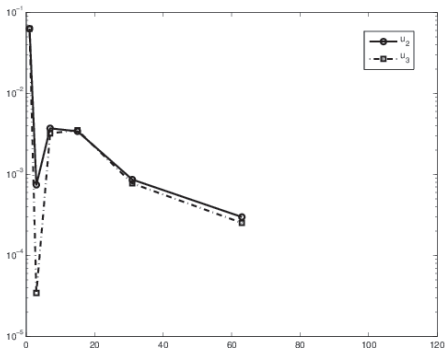


Figure: Errors on mean value (left) and variance (right) versus number of grid points

The flux entering a fracture  $F_2$  or  $F_3$  can be modelled as follows:

$$u(y) = u_S(y) + \varepsilon u_R(y) ,$$

where

- (S for *smooth*)  $u_S$  is the smooth part (large-scale behaviour)
- (R for *rough*)  $u_R$  is the rough part (small-scale behaviour)

whereas  $\varepsilon > 0$  is a small parameter.

Let us assume (just for convenience of the analysis) *periodicity* in the  $y$ -variable.

Assume that  $u_S$  is *analytic* in a strip in the complex plane containing the real axis, and admits an expansion of the form

$$u_S(y) = \sum_{k \geq 0} (a_k \cos ky + b_k \sin ky) ,$$

with

$$|a_k| \sim |b_k| \sim e^{-\alpha k}$$

for some  $\alpha > 0$ .

Then, for the  $L^2$ -projection

$$P_J u_S = \sum_{k=0}^J (a_k \cos ky + b_k \sin ky)$$

we have an *exponential* decay of the error as  $J \rightarrow \infty$ :

$$\|u_S - P_J u_S\|_{L^2(0,2\pi)}^2 \lesssim \frac{1}{\alpha} e^{-2\alpha J} .$$

On the other hand, assume that the rough component  $u_R$  has the form of a *shifted and scaled square wave*

$$u_R(y) = \frac{1}{M} w(My),$$

where  $M > 0$  is an integer and  $w = w(t)$  is the *square wave*

$$w(t) = \begin{cases} 1 & \text{if } 2k\pi < t < (2k+1)\pi \\ -1 & \text{if } (2k+1)\pi < t < (2k+2)\pi. \end{cases} \quad \text{for some } k \in \mathbb{Z},$$

The Fourier expansion is

$$u_R(y) = \frac{2}{\pi} \sum_{m \geq 0} \frac{1}{(2m+1)M} \sin((2m+1)My) =: \sum_{k \geq 0} c_k \sin ky,$$

with

$$c_k = \begin{cases} \frac{2}{\pi k} & \text{if } k = (2m+1)M \text{ for some } m \geq 0, \\ 0 & \text{elsewhere.} \end{cases}$$

Thus,

$$\|u_R - P_J u_R\|_{L^2(0,\pi)}^2 \sim \frac{2}{\pi M} \frac{1}{J}.$$

For the model flux  $u = u_S + \varepsilon u_R$ , we have the Fourier expansion

$$u(y) = \sum_{k \geq 0} (a_k \cos ky + \tilde{b}_k \sin ky) ,$$

with  $\tilde{b}_k := b_k + \varepsilon c_k$ . Note that

$$\tilde{b}_k = b_k \quad \text{whenever} \quad k \neq (2m + 1)M \text{ for any } m \geq 0,$$

thus in particular the Fourier coefficients of  $u$  corresponding to the first  $M$  modes coincide with those of  $u_S$ , hence they decay at an exponential rate.

The  $L^2$ -approximation error satisfies

$$\|u - P_J u\|_{L^2(0, 2\pi)}^2 \leq \begin{cases} \frac{4}{\alpha} e^{-2\alpha J} & \text{for all } J \leq J_* , \\ \frac{8\varepsilon^2}{\pi M} \frac{1}{J} & \text{for all } J > J_* . \end{cases}$$

for a suitable  $J_* = J_*(\alpha, \varepsilon, M)$ .

Thus, the larger is  $M$  (which in our application could be related to the number of fractures), the larger is the value of  $J$  for which one “sees” an exponential convergence.

- Consider log-normal distributions as well
- Increase the number  $N$  of fractures in the network
- Attribute random orientation to fractures via a K-L expansion
- Furtherly increase the stochastic dimensionality  $M$  by randomizing other relevant parameters of the network: density of fractures, characteristic length, aspect ratio...
- Provide a rigorous mathematical analysis of the dependence of quantities of interest (e.g., output fluxes) from the random variables.
- Inject adaptivity in the UQ process.